Journal of Materials Chemistry A

Accepted Manuscript

ROYAL SOCIETY OF CHEMISTRY

www.rsc.org/materialsA

Graphical Abstract

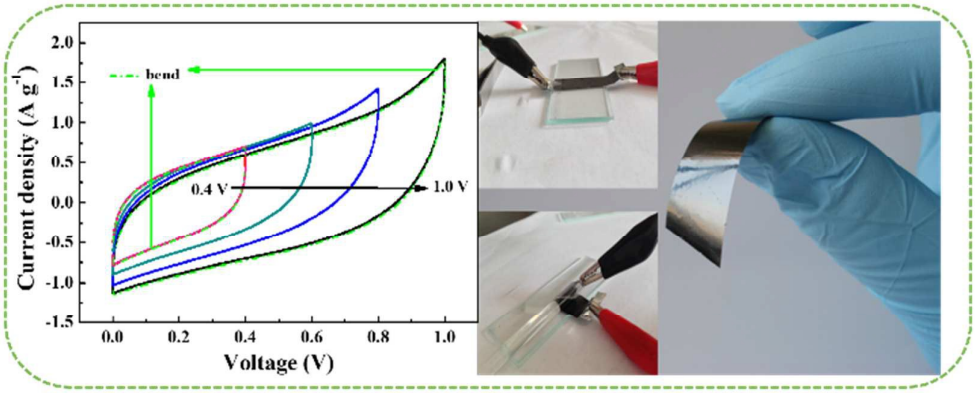

Journal of Materials Chemistry A

PAPER

Preparation of Two-Dimensional Flexible MnO_2/Graphene Thin Film and its application in Supercapacitor

Received xxth xxxxxxxx 20xx,
Accepted xxth xxxxxxxx 20xx

DOI: 10.1039/x0xx00000x

www.rsc.org/

Zhimin Li, Yufeng An, Zhongai Hu,* Ning An, Yadi Zhang, Bingshu Guo, Ziyu Zhang, Yuying Yang and Hongying Wu

Novel two-dimensional (2D) free standing and flexible MnO_2/graphene film (MGF) supercapacitor electrode is successfully fabricated by the spin-coating and hydrothermal process. The MnO_2 nano-sheets are properously aligned vertically only on one side of the graphene thin film. Raw amphiphilic graphene oxide film is helpful in effectively promoting the dispersion of well-defined MnO_2 nanosheets, which can form porous network and cover the film surface. The gaphene film act as a substrate where MnO_2 nano-sheets grew in situ, and meanwhile it is used as a base current collector with a large accessible surface area and without binders for the electrochemical testing. The MGF exhibits excellent electrochemical performance in the three electrode configuration, including a high specific capacitance up to 280 F g^{-1} and outstanding cycle stability (no obvious decay after 10000 cycles). In addition, the symmetric MGF supercapacitor shows a specific capacitance up to 77 F g^{-1} under a cell voltage of 1.0 V. After 10000 cycles, the capacity retention rate is 91% at a current density 1 A g^{-1}. At the same time, the symmetric supercapacitor also get high energy density of 10.7 Wh kg^{-1} at a power density of 500 W kg^{-1}.

1. Introduction

In recently, some flexible electronic sets have been reported, such as bendable mobile phones, wearable devices and portable displays. [1-4] It's amazing that a phone screen can be bendable, however, the energy storage unit can't do this better until now. In contrast, most of the energy storage devices, such as supercapacitors, are usually too heavy, bulky and apparently rigid for much of the special requirement of a flexible electronic set: small, soft and light. Therefore, it's meaningful to explore the new generation of supercapacitor with flexible, light, free-standing and nano-units thin film electrode materials.[5] As for supercapacitors, the charge storage mechanisms are mainly classified as electrical double-layer capacitors (EDLs) and pseudocapcitors.[6-8] In spite of having high power density and long life cycle, EDLs suffered from relatively low energy density. In EDLs, the capacitance arises from the charge separation at the electrode/electrolyte interface. Therefore, the interface material selection is extremely important and carbon materials are always preferred. Graphene and carbon nanotubes (CNTs) were employed as desired carbon materials due to their superior electrical conductivity, high electrochemical and good mechanical properties.[9] Pseudocapcitor is a different kind of supercapacitor, in which the psedocapcitance arises from faradic reactions occurring at the electrode/electrolyte interface. As a result, pseudocapcitors exhibit higher specific capacitance and energy density than EDLs. Unfortunately, the poor cycle ability has restricted the further application of pseudocapcitors. [10]

The pseudocapcitor materials are mainly including transition-metal oxides and conducting polymers. As a typical transition metal oxide, MnO_2 attracted much attention because of its abundance, low cost, environmental friendly, rich redox activity and high theoretical specific capacitance (1232 F g^{-1}).[11-14] In order to overcome its poor electrical conductivity and the cycling crystal expansion/contraction induced flaking off during repeated cycling processes, the conducting carbon materials such as graphene and CNTs were used as supporting materials.[15-18] Recently, several interesting MnO_2-carbon based composites have been reported. For instance, Teng et *al*. prepared MnO_2 /CNTs composite by MnO_2 nanoparticles growing on CNTs under in-situ hydrothermal conditions. The obtained composite has shown specific capacitance of 125 F g^{-1}.[19] Wang et *al*. prepared MnO_2/CNT composite by a facile direct redox reaction. The composite has shown specific capacitance of 162.2 F g-1 at the current density of 0.2 A g^{-1}.[20] MnO_2/graphene composites have also been investigated for full available of MnO_2. Qian et *al*. have fabricated a three dimensional porous graphene-MnO_2 composites via deposition of MnO_2 particles on graphene from freeze-drying method and obtained a specific capacitance of 800 F g^{-1} at the current density of 0.1 A g^{-1}.[21] Ghasemi et al. have discussed the type of substrate and the preparation method of inflorescence to MnO_2/graphene composites specific capacitance. Their research has shown that the special capacitance of MnO_2/electrochemically reduced graphene oxide/stainless steel (MnO_2/ERGO/SS) was higher than electrochemically reduced graphene oxide/stainless steel (ERGO/SS).[22]

*Key Laboratory of Eco-Environment-Related Polymer Materials of Ministry of Education, Key Laboratory of Polymer Materials of Gansu Province, College of Chemistry and Chemical Engineering, Northwest Normal University, Lanzhou, Gansu 730070, China. Fax: +86 931 8859764; Tel.: +86 931 7973255; E-mail: zhongai@nwnu. edu.cn

With the explosive growing of the portable electronic devices, such as mobile phone and wearable devices, flexible and free-standing MnO_2-based electrode materials for supercapacitors have emerged. Recently, Chou et *al*. have reported that MnO_2 nanowire/CNT composite paper (MNCCP) can be used as a flexible electrode for electrochemical supercapacitor. They have found that MNCCP electrode displayed specific capacitance as 167.5 F g^{-1} at a current density of 77 mA g^{-1}.[23] Guo et al. have fabricated a self-standing MnO_2/graphene porous film without binder by a hard template method and hydrothermal process. The test result showed that the film revealed the specific capacitance up to 266.3 F g^{-1} at the current density of 0.2 A g^{-1}.[24] The graphene/CNTs/MnO_2 nanocomposite plus CNTs (GMC+C) electrode fabricated by Hung et *al*. with electrophoretic deposition method showed an excellent specific capacitance of 964 F g^{-1} due to low ion/electron transport resistances and short ion/electron diffusion lengths.[25] These pioneer works have shown that the combination of MnO_2 and carbon materials is a highly valuable alternative pathway to improve the specific capacitance behavior of MnO_2 based electrode. As a proverbial carbon material, graphene has high specific surface area and superior electrical conductivity, more important, it's flexible. So it is reasonable to use MnO_2-graphene combination as a potential electrode material for fabricating flexible supercapacitors to meet the demands of portable electronic devices.

As our continuous interesting on supercapacitor fabrication and investigation, here we present a novel flexible thin MGF film electrode based on MnO_2-graphene combination composites. In this work, the MnO_2 nanosheets have been planted only on one side of graphene film without any binders. It's well known that active materials, current collector and binder are essential parts for fabricating a supercapacitor. In the MGF, a large specific surface provided by graphene film makes the usage of large psedocapacitance of MnO_2 possible. At the same time, the graphene film also acts as a fast electrotransport current collector without binders. The MnO_2 nanosheets vertically aligned on the graphene surface forming an open porous structure. Therefore, the electrons of MnO_2 surface can across a much shorter distance to the current collector. As a result, the interface between MnO_2-graphene film electrode and the electrolyte increased greatly. The experiment result shown that the flexible MGF as supercapacitor electrodes with high capacitance of 280 F g^{-1} at 1 A g^{-1}, after 10000 cycles the capacitance content is 99%. A further studies showed that a flexible MGF applied symmetric supercapacitor has provided a 77 F g^{-1} capacitance at current density of 1 A g^{-1}, and the capacitance content kept at 91% after 10000 cycles, the energy density is 10.7 Wh kg^{-1} at the power density of 500 W kg^{-1}. To our knowledge, this kind of combined graphene film acting as a current collector has never been reported.

2. Experimental

2.1. Materials

$KMnO_4$ and EtOH were purchased from Sigma-Aldrich and were used as received. Deionized water was used throughout all the experiments.

2.2. Preparation of MGF

Graphite oxide (GO) was synthesized from powered flake graphite by modified Hummers method. [26]. The MGF preparation procedure as follow (Fig1): (1) Spin-coating: Raw GO film was constructed by spin-coating with graphene oxide colloid solution (0.5 mg mL^{-1}) obtained by ultrasonic dispersion: First, graphene oxide colloid solution (every drop contain about 0.1ml colloid solution) was dropped on a rotating quartz plate at the 1200 revolutions per minute, then the plate was irradiated by an infrared lamp at 45 °C for 20 seconds. The described spin-coating process was repeated for 12 times in order to meet the thickness and mechanical strength requirements of laboratory operations. (2) Hydrothermal process: $KMnO_4$ (100 mg) was dissolved in deionized water (100mL) and then EtOH (2 mL) was added. After the mixture was stirring for 30 minutes, the GO film (fixed by several pieces of quartz plate) with quartz plate was dipped in the mixture and heated to 140 °C for 12 hours by hydrothermal process. GO film can partly function as supporting substrate and sacrificial reductant to form the MnO_2-graphene film, because the C atoms of GO can reduce Mn^{7+} to Mn^{4+}. The reaction mechanism is proposed as follows: [27]

$$4KMnO_4 + 3C + H_2O \longrightarrow 4MnO_2 + 2KHCO_3 + K_2CO_3$$

The reduction process triggered the formation of MnO_2 nanoparticles on graphene film surface and further expanding on the film. (3) MGF stripping: After the hydrothermal process, one of the corners of the formed MGF was peeled carefully, then the quartz plate was inclined and dipped in water slowly. The film was peeling off little by little as a result of the surface tension. After several times washing, the film was fished out by a platinum net and dried gently with N2. The formed thin film were then stripped and washed with deionized water and ethanol for several times, and vacuum dried at 80 °C for 12 h (Fig. 1). For comparison, the pure rGO film was also prepared by the same procedure but the $KMnO_4$ was absent. As expected, bulk MnO_2 was formed instead of GO film.

2.3. Characterization of MGF

The morphology of rGO film and the MGF were characterized by Zeiss Ultra Plus field-emission scanning electron microscopy (FESEM) at an operating voltage of 5 kV. Transmission electron microscopy (TEM) images were acquired on an FEI TECNAI G2 F20 STWIN D2278 microscope at 200 kV. Fourier transformed infrared (FTIR) spectra were recorded on a Nicolet Nexus 470 spectrometer. Wide-angle X-ray diffraction (XRD) analyses were carried out on a PANalytical X'pert PRO X-ray diffractometer with Cu Kα radiation. The elementary composition was determined using a Thermo ESCALAB 250XI photoelectron spectroscopy (XPS). Thermogravimetric (TG) analysis was carried out using a Perkin-Elmer TG/DTA-6300 instrument in the temperature range of 20-600 °C at heating rate of 5 °C min^{-1} under air atmosphere.

2.4. Electrochemical measurement

The working electrode was prepared by cutting MGF thin film into pieces and used directly. Single film electrochemical analyses were performed using a three-electrode system equipped with an SCE reference electrode and a platinum counter electrode. A symmetric supercapacitor application was also fabricated: a polypropylene film was used as separator between two pieces of the MGF films in 1M Na_2SO_4 electrolyte to build a cell. All of the electrochemical measurements including cyclic voltammetry (CV), galvanostatic charge-discharge (GCD), and electrochemical impedance

spectroscopy (EIS) were carried out using an electrochemical workstation CHI660D.

The specific capacitance (*C*, F g^{-1}) was obtained from the discharge process according to the following equation: [28]

$$C = \frac{i \cdot t}{\Delta V \cdot m} \quad (1)$$

where *i* is the discharging current (A), *t* is the discharge times (s), Δ*V* is the potential change during discharge process, and *m* is the mass of composite.

The total capacitance (*C*, F g^{-1}), power density (*P*, kW kg^{-1}), and energy density (*E*, Wh kg^{-1}) of the cell was calculated from the galvanostatic charge-discharge curves by the formula (1), (2) and (3): [29]

$$E = \frac{0.5C \cdot (\Delta V)^2}{3.6} \quad (2)$$

$$P = \frac{3600E}{t} \quad (3)$$

where *i* (A) is the discharge current, *t* (s) is the discharge time, Δ*V* (V) is the applied cell voltage.

3. Results and discussion

The physical and electrochemical performances of the MGF have been studied and discussed.

3.1. Characterization

Fig. 2(a) has shown that the MGF is large enough to be used as a laboratory electrode for electrochemistry behavior test. A flexible supercapacitor set constructing by the MGF has flexible and free-standing properties as shown in Fig. 2(b). Moreover, there is no cracking of the bending MGF in the symmetric supercapacitor as shown in the inset of Fig. 2(b).

The dispersion and morphology of MnO_2 on rGO film was examined by FESEM and TEM technology. It was found that the surface of pure rGO film shows special crinkle (Fig. 3(a)). While the surface situation of the rGO film was changed after the MGF preparation process, the MnO_2 nanopaiticles covered up all over the rGO film surface (Fig. 3(b)). Surprising, the more detail observation shows MnO_2 nanosheets were formed and the MnO_2 nanosheets vertically grew up along the graphene surface and constructed a porous network structure (Fig. 3(c)). Fig. 3(d) shows the FESEM image of cross section of rGO film, it's clear that the rGO film has a layer-bylayer structure and the average thickness of it is about 3 μm. Meanwhile, it is seen from the FESEM images of cross section of MGF (Fig. 3(e) and (f)), that the rGO film was covered by MnO_2 sheets only on one side. The thickness of MnO_2 layer is about 50 nm~200 nm. The MnO_2 nanosheets stacked with each other and formed a porous network, which will benefit the transport of ion toward the surface of electrode material. The packaging space between MnO_2 nanosheets act as ion buffer "reservoir" for electrolyte (Fig. 4(a)). It is thought that the fine morphology comes from a good substrate, that is, rGO thin film. Because a good rGO thin film, with smooth, continuous and large area, can prevent the insoluble MnO_2 agglomeration. This can be proved by the TEM image of pure rGO film in Fig. 4(b), which have a smooth, continuous and large area grapheme film. The following growth of MnO_2 sheet on the rGO film confirmed this again. The MnO_2 sheet exhibits a uniform and tight pattern (Fig. 4(c)). The particles size of MnO_2 sheets consistent with that of FESEM characterization (Fig. 4(d)).

The XRD patterns of the MGF and pure rGO film confirmed the formation of MnO_2 network on the rGO film (Fig. 5(a)). The diffraction peaks of the MGF are similar to α-MnO_2 (JCDS No. 44-0141), and agree well with the reported MnO_2 on graphene.[30-32] Furthermore, the diffraction peak at around 24° is attributed to the (002) crystal plane of rGO, which almost disappeared in the MGF as a result of MnO_2 nanosheets homogeneous covered the rGO film surface.

Detailed surface information of the MGF was collected by X-ray photoelectron spectroscopy (XPS) and the corresponding results are presented in Fig. 5(b). The existence of elements Mn elucidates the MnO_2 is successfully formed on the surface of rGO film. The deconvoluted Mn 2p core-level spectra of the MGF in Fig. 5(c) show the peaks of Mn $2p_{3/2}$ and Mn $2p_{1/2}$ is located at 642.6 eV and 654.2 eV, respectively. The consistent spin-energy separation value between the Mn $2p_{3/2}$ peak and the Mn $2p_{1/2}$ peak is 11.6 eV. These results are in accordance with previous works about Mn $2p_{3/2}$ and Mn $2p_{1/2}$ in MnO_2.[33-35]

FT-IR analysis of the MGF was shown in Fig. 5(d). The absorption band at 3415 cm^{-1}, 1635 cm^{-1} and 1060 cm^{-1} can be assigned to aromatic O-H, C-C and C-O stretching vibrations. These functional groups can help the MnO2 bonding to rGO film via hydrogen bonds.[36, 37] The peaks located at 723cm^{-1} and 532 cm^{-1} in the spectra of the MGF can be ascribed to the Mn-O-Mn and Mn-O vibrations. Importantly, the typical C-O absorption bands at 1730 cm^{-1} was almost disappeared, suggesting that the carbonyl groups at the surface of the GO films are substituted by MnO_2.[38] The MGF was also analyzed by TGA as shown in Fig. 5(e). The film was heated from room temperature to 700 °C at 5 °C min^{-1}. The first weight loss up to 120°C attributed to removal constituent water molecules. The gradual weigh decrease after that until reached 350 °C was assigned to the decomposition of the oxygen-containing functional groups at the surface of rGO film, and the removal of the functional groups bonded with MnO_2 at the hydrothermal treatment.[39] In the temperature range 350-480 °C, the carbon skeleton of rGO films was burned up.[40] The small weight loss above 435 °C is related to phase transformation of MnO_2.[41] Which helped to determine the mass ratio of MnO_2 in the MGF as 67%.

The above investigations has shown that specific structure of the MGF not only prevented the aggregation and restacking of MnO_2 nanosheets and in favor of the vertical growth of MnO_2 nanosheets on the flat surface of graphene and forming a regular network, but also provided a huge surface area of MnO_2 contacting with electrolyte and improved the pseudocapacitance reaction active sites. Additionally, the MGF electrode can effectively improve the pseudocapacitance energy density through elide the binder and current collector. These effects indicate that MGF is a great candidate as an efficient electrode material for supercapacitors fabrication. In this work, the MGF electrochemical performance was investigated in 1M Na_2SO_4 aqueous solution by a three-electrode system. Moreover, the supercapacitors electrochemical performance was tested through two electrodes system.

3.2. Three-electrode system

A three-electrode system CV curves were measured at scan rate 10 mV s^{-1} within a potential window of 0 to 0.9 V vs. SCE (Fig. 6(a)). The pure rGO film shows approximately rectangular shape of CV curve, which is characterized as an electrical double layer (EDL) capacitor. The CV curve of the MnO_2 shows basically rectangular shapes due to the fast and reversible successive surface redox reactions of MnO_2 phase. This kind of CV is the typical pseidocapacitive behavior in a neutral electrolyte. As for the CV curve of the MGF, it exhibits rectangular shape with weak redox peaks which is comparable with the reported MnO_2-carbon composite. These electrochemistry investigations proved MnO_2 in the MGF is a favorable substitute for RuO_2 in the application of supercapacitors, not only because it is cheaper but it has similar charge storage mechanism as hydrous RuO_2. The MnO_2 charge storage mechanism is demonstrated as below:[42]

$$MnO_2 + xMn^+ + yH^+ + (x+y)e^- \longleftrightarrow MnOOM_xH_y$$

In the reaction formula, MnO_2 exhibits fast charge-discharge capability and analogous to non-Faradaic energy storage behavior based on surface adsorption of electrolyte cations M^+ (Na^+, K^+ et *al*.) as well as proton incorporation. Even more, the MnO_2 nano-sheets vertically arranged on rGO film, which minimized the contact resistance and allowed easier Faraday processes of the electrochemical active materials. At the same scanning rate, the observed CV loop of the MGF much larger than rGO film and pure MnO_2, which consistence with the larger specific capacitances of MGF. The dramatic enhancement of the specific capacitance of MGF can be attributed to the synergistic effect between the conductive carbon material rGO and pseudocapactive material MnO_2. The synergistic effect comes from the special structure of the MGF, which provided more diffusion pathways than bulk MnO_2 and rGO film for the fast ion transport and facile charge storage. The MGF, rGO film and bulk MnO_2 galvnostatic charge-discharge curves at 1 A g^{-1} has shown that the MGF with weak plateau corresponds with the results in the CV curves (Fig. 6(b)). The specific capacitance values of the MGF calculated from the discharge curves according to the Eq. (1) is 280 F g^{-1}, which is much higher than rGO film (31 F g^{-1}) and bulk MnO_2 (108 F g^{-1}). As shown in Fig. 6(c), the CV curve of MGF still retained a similar shape at high sweep rate, which indicated that the MGF has an excellent capacitance behavior and there existed fast diffusion paths for electrolyte ions diffusion into the MGF. At different specific currents, the GCD curves of the MGF have shown that all of the curves are close to an isosceles triangle due to the intrinsic reversibility of the MGF (Fig. 6(d)). When the current density are 1, 2, 3, and 5 A g^{-1}, the specific capacitances are 280, 196, 168 and 135 F g^{-1}, respectively. At the same time, specific capacitance retention of 49% is achieved as specific current is increased from 1 to 5 A g^{-1}.

Typical complex plane plots for the MGF, rGO film and MnO_2 are presents in Fig. 7(a), the frequency ranged from 0.1 Hz to 5 kHz at a bias of 0.4 V (vs. SCE) reference electrode. The complex plane plots for the MGF and MnO_2 were all containing a small and semicircle loop at high frequency, which implied both of them have electrochemical activity. The diameter of the semicircle is corresponding to the charge transfer resistance (R_{ct}.) at the electrode/electrolyte interface. The MGF has exhibited smaller R_{ct} than bulk MnO_2, which may be attributed to the specific constructer of the MGF. The nano-sheets of MnO_2 were vertically embedded on rGO film and formed a porous network. This type of structure has facilitated the transportation of the electrolyte to the electrode and helped to reduce the R_{ct} in the MGF. In the low-frequency region, the slope of the straight line indicates the diffusive resistance of the electrolyte to the electrode constructer. Compared with the MnO_2, the MGF's slope of straight line is bigger, suggesting it has lower diffusive resistance of the electrolyte and faster ion transport speed.

To evaluate the stability of the MGF during the charge-discharge circles, the specific capacitance as a function of charge-discharge cycle numbers at 3 A g^{-1} in 1M Na_2SO_4 aqueous solution were exhibited in Fig. 7(b). Both of the MGF and rGO film have shown better cyclic stability than the bulk MnO_2, but the specific capacitance of rGO film is far less than the MGF. It is clearly that the MGF puts up better performance in terms of specific capacitance and cycle stability compared with rGO and MnO_2. The specific capacitance of the MGF was increasing during the first 600 cycles, which indicates that a so-called activated process was needed to full relief the MGF pseudocapacitance. After such an electrochemical activation, the specific capacitance is kept still at the following cycles without obvious decay (about 99% of initial value). This result is better than the other kinds of MnO_2/graphene electrodes, in which, 5 to 20% degradation of the specific capacitance in 500 to 2000 cycles was observed.[7, 22] The high capacitance and a long cycle life of MGF can be attributed to the MnO_2 nanosheets tightly attached to the rGO surface and kept up the stability to avoid the material structure collapse on cycling. In addition, the porous nanostructure of MnO_2 nanosheets can accommodate a large number charge during cycling, while the rGO film was used as conductive current collector. When the MnO_2 nanosheets were covered on the rGO film without binder, the Faradaic charging and discharging process was promoted dramatically.

3.3. Two-electrode system

To as a continuous work, a symmetric two-electrode cell was fabricated to examine the actual performance of the MGF as electrode material for supercapacitors. The CV curves of the supercapacitor at different cell voltages ranging from 0.4 V to 1.0 V at 15 mV s^{-1} were shown in Fig. 8(a). It is clearly that the assembled supercapacitor exhibits an ideal capacitive behavior with quasi-rectangular CV curves within whole operating voltage. When the symmetric two-electrode cell was bending, there is no significant change of the CV curves, which means the MGF has excellent flexible characteristics. The CV curves still retain a relatively rectangular shape without obvious change when the scan rate was increasing from 10 to 200 mV s^{-1} as shown in Fig. 8(b), indicting a fast charge-discharge property of the cell. The specific capacitance of the MGF in two-electrode system are estimated from galvanostatic discharge cures at the different current densities 1, 2, 3 and 5 A g^{-1} were shown in Fig. 8(c). It should be noted that the specific capacitance was calculated using the total mass of the MGFs on the two electrode, the calculated maximum specific capacitance is 77 F g^{-1} at 1 A g^{-1}. When the current density was increased to 5 A g^{-1}, the symmetric supercapacitor still retained about 46% specific capacitance of the current density at 1 A g^{-1}, indicating good rate capability of this device. The long-term cycle stability of the supercapacitor was also examined using the charge-discharge measurements conducted at 1 A g^{-1} over 10000 cycles

(Fig. 8(d)). A capacitance retention ratio 91% was obtained after the cycles. Compared to single electrode, the cycle stability of as-assembled device has a little decline, which may be ascribed to the loss of electrolyte. However, the result is still superior to other reported as-assembled devices. [32, 43-45] In addition, the energy density and power density of the cell can be calculated according to the Equ. (2) and (3). The full cell reached an energy density of 10.7 Wh kg^{-1} at the power density of 500 W kg^{-1}. The Ragone plot of as-assembled supercapacitor in Fig. 8(e) has shown that the divice in this work has a good performance compared with some similar flexible symmetric supercapacitor, such as MnO_2/3D-PC (6.6 Wh kg^{-1}),[32] graphene/MnO_2 (3.74 Wh kg^{-1}),[43] PPy/GO/ZnO (10.65 Wh kg^{-1}),[44] graphene/MnO_2/CNT (3.2 Wh kg^{-1}),[45] N-CNFs-900 (6.5 Wh kg^{-1}),[46] and CNTs@Mn-MOF (6.6 Wh kg^{-1}).[47] These results indicate that the MGF is an excellent electrode material for potential application in flexible supercapacitors device.

4. Conclusion

A flexible MGF thin film was successfully prepared by spin-coating and hydrothermal process was used as supercapactor electrodes. The flexible MGF exhibited high specific capacitance and cyclic stability. The MnO_2 nanosheets formed a porous network and vertically attached along only one side of the rGO film, this kind of structure improved the cyclic stability of MnO_2 dramatically and good ionic and electronic transport ability in the film matrix. Moreover, when the MGF was applicated in a supercapacitor device, no binder is needed and the current collector is rGO film, this will reduce the device weight and improve the energy density and power density of the cell significantly. It's reasonable to believe that as an electrode material the flexible MGF is a promising candidate for supercapacitors fabrication.

Acknowledgements

We gratefully acknowledge the financial support offered by the National Natural Science Foundation of China (Nos. 20963009, 21163017 and 21563027), Specialized Research Fund for the Doctoral Program of Higher Education (No. 20126203110001), and the Natural Science Foundation of Gansu Province, China (No. 1308RJZA261).

References

1 B. Siegfried, *Nat. Mater*, 2013, **12**, 871-872.
2 A. Russo, B.Y. Ahn, J.J. Adams, E.B. Duoss, J.T. Bernhard, J.A. Lewis, *Adv. Mater*, 2011, **23**, 3426-3430.
3 A. Nathan, A. Ahnood, M.T. Cole, S. Lee, *P. IEEE*, 2012, **100**, 1486-1517.
4 Y. Sun, J.A. Rogers, *Adv. Mater*, 2007, **19**, 1897-1916.
5 X. Wang, X. Lu, B. Liu, D. Chen, Y. Tong, G. Shen, *Adv. Mater*, 2014, **26**, 4763-82.
6 L. Bao, J. Zang, X. Li, *Nano Lett.*, 2011, **11**, 1215-1220.
7 S. Bose, T. Kuila, A.K. Mishra, R. Rajasekar, N.H. Kim, J.H. Lee, *J. Mater. Chem.*, 2012, **22**, 767-784.
8 H.W. Liang, Z.Y. Wu, L.F. Chen, C. Li, S.H. Yu, *Nano Energy*, 2015, **11**, 366-376.
9 P. Martin, *Chem. Soc. Rev.*, 2010, **39**, 4146-57.
10 D. Zhang, Z. Xiong, C. Yao, Y. Peng, C. Wang, Y. Ma, *J. Power Sources*, 2011, **196**, 5990-5996.
11 K. Shimamoto, K. Tadanaga, M. Tatsumisago, *Electrochim. Acta*, 2013,**109**, 651-655.
12 Y. Xiao, M. Cao, *ACS Appl. Mater. Inter*, 2015, **23**, 12840-12849.
13 C. Fang, D. Zhang, S. Cai, L. Zhang, L. Huang, H. Li, P. Maitarad, L. Shi, R. Gao, J. Zhang, *Nanoscale*, 2013, **5**, 9199-9207.
14 S. Cai, H. Hu, H. Li, L. Shi, D. Zhang, *Nanoscale*, 2016, **8**, 3588-3598.
15 J. Li, X. Cheng, A. Shashurin, M. Keidar, *Graphene*, 2012, **01**, 1-13.
16 G. Zhao, X. Huang, X. Wang, P. Connor, J. Li, S. Zhang, J. T. S. Irvine, *J. Mater. Chem. A*, 2015, **3**, 297-303.
17 J. Mei, L. Zhang, *Materials Letters*, 2015, **143**,163-166.
18 L. Li, Z.A. Hu, N. An, Y.Y. Yang, Z.M. Li, H.Y. Wu, *J. Phys. Chem. C.*,2014, **40**, 22865-22872.
19 F. Teng, S. Santhanagopalan, D.D. Meng, *Solid State Sci.*, 2010, **12**, 1677-1682.
20 H. Wang, C. Peng, F. Peng, H. Yu, J. Yang, *Mater. Sci. Eng. B*, 2011, **176**, 1073-1078.
21 Q. Lei, L. Lu, *Colloid*. *Surface A,* 2015, **465**, 32-38.
22 S. Ghasemi, R. Hosseinzadeh, M. Jafari, Int. *J. Hydrogen Energ.*, 2015, **40**, 1037-1046.
23 S.L. Chou, J.Z. Wang, S.Y. Chew, H.K. Liu, S.X. Dou, *Electrochem. Commun.*, 2008, **10**, 1724-1727.
24 W.H. Guo, T.J. Liu, P. Jiang, Z.J. Zhang, *J. Colloid. Interf. Sci*, 2015, **437**, 304-10.
25 C.J. Hung, P. Lin, T.Y. Tseng, *J. Power Sources*, 2014, **259**, 145-153.
26 W.S. Hummers, R.E. Offeman, *J. Am. Chem. Soc.*, 1958, **80**, 1339.
27 M. Kim, Y. Hwang, J. Kim, *J. Power Sources*, 2013, **239**, 225-233.
28 Z. Li, Y. Su, G. Yun, K. Shi, X. Lv, B. Yang, *Solid State Commun.*, 2014, **192**, 82-88.
29 Z. Wu, W. Ren, D. Wang, F. Li, B. Liu, H. Cheng, *ACS Nano*, 2010, **4**, 5835-42.
30 M. Pang, G. Long, S. Jiang, Y. Ji, W. Han, B. Wang, X. Liu, Y. Xi, *Sci. Eng. B* ,2015,**194**, 41-47.
31 J. Liu, *J. Mater. Chem*, 2012, **22**, 2419-2426.
32 L.Wang, Y. Zheng, S. Chen, Y. Ye, F. Xu, H. Tan, L. Zhuang, H. Hou, Y. Song, *Electrochim. Acta*, 2014, **135**, 380-387.
33 T. Gan, Z. Shi, Y. Deng, J. Sun, H. Wang, *Electrochim. Acta*, 2014, **147**, 157-166.
34 C. Liu, D. Gui, J. Liu, *Chem. Phys. Lett.*, 2014, **614**, 123-128.
35 J. Mei, L. Zhang, *Electrochim. Acta*, 2015, **173**,338-344.
36 K.R. Nemade, S.A. Waghuley, *J. Lumin.*, 2014, **153**, 194-197.
37 M. Kim, Y. Hwang, J. Kim, *Chem. Eng. J.*, 2013, **230**, 482-490.
38 J. Qu, L. Shi, C. He, F. Gao, B. Li, Q. Zhou, H. Hu, G. Shao, X. Wang, J. Qiu, *Carbon*, 2014, **66**, 485-492.
39 Y. Liu, D. Yan, R. Zhuo, S. Li, Z. Wu, J. Wang, P. Ren, P. Yan, Z. Geng, *J. Power Sources*, 2013, **242**, 78-85.
40 G.F. Chen, Z.Q. Liu, J.M. Lin, N. Li, Y.Z. Su, *J. Power Sources*, 2015, **283**, 484-493.
41 S. Sun, P. Wang, S. Wang, Q. Wu, S. Fang, *Mater. Lett.* , 2015, **145**, 141-144.
42 Y. Wang, Y. Liu, I. Zhitomirsky, *J. Mater. Chem. A*, 2013, **1**, 12519-12526.
43 Y. He, W. Chen, X. Li, Z. Zhang, J. Fu, C. Zhao, E. Xie, *ACS Nano*, 2012, **7**, 174-182.

44 W. K. Chee, H. N. Lim, I. Harrison, K. F. Chong, Z. Zainal, C. H. Ng, N. M. Huang, *Electrochim. Acta*, 2015, **157**, 88-94.
45 Y. Cheng, S. Lu, H. Zhang, C. V. Varanasi, J. Liu, *Nano Lett*, 2012, **12**, 4206-4211.
46 L. Chen, X. Zhang, H. Liang, M. Kong, Q. Guan, P. Chen, Z. Wu, S. Yu, *ACS Nano*, 2012, **6**, 7092-7102.
47 Y. Zhang, B. Lin, Y. Sun, X. Zhang, H. Yang, J. Wang, *RSC Adv*, 2015, **5**, 58100-58106.

Figure Captions

Fig.1. The preparation of MGF by spin-coating and hydrothermal process**.**

Fig. 2. Photograph of (a) the size of MGF and (b) the flexible shows of MGF.

Fig. 3. FESEM images: top view of (a) bare rGO film, (b) and (c) MGF; cross section of (d) bare rGO film, (e) and (f) MGF.

Fig. 4. (a) High FESEM of the MGF (b) TEM of rGO (c) TEM of the MGF (d) size of MnO_2.

Fig. 5. (a) XRD pattern of the MGF and rGO film (b) XPS wide scan survey spectra (c) XPS Mn 2P spectrum of MGF (d) FT-IR spectra (e) TGA curve.

Fig. 6. (a) CVs of the MGF, MnO_2 and rGO film at the scan rate of 10 mV s^{-1}. (b) MGF, MnO_2 and rGO film GCD curves at 1 A g^{-1}. (c) MGF at various scan rates, (d) GCD curves of the MGF at different specific currents.

Fig. 7. (a) Nyquist plots of the rGO film, bulk MnO_2 and MGF, (b) the cycle lifetime of MGF, bulk MnO_2 and rGO film.

Fig. 8.(a) CV curves of bending or normal MGF in a two-electrode cell configuration with different cell voltages at a scan rate of 15 mV s^{-1}, (b) CV curves at various scan rates within the operating voltage of 1.0 V, (c) discharge curves at different current densites , (d) cycle lifetime of full cell at 1 A g^{-1} and (e) Ragone plot of as-assembled supercapacitor.

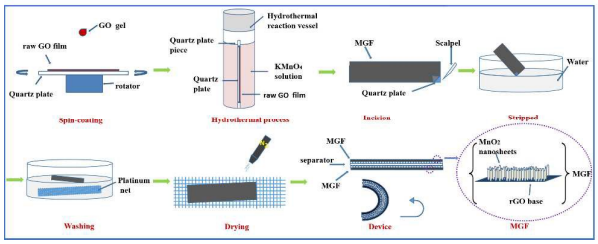

Fig. 1

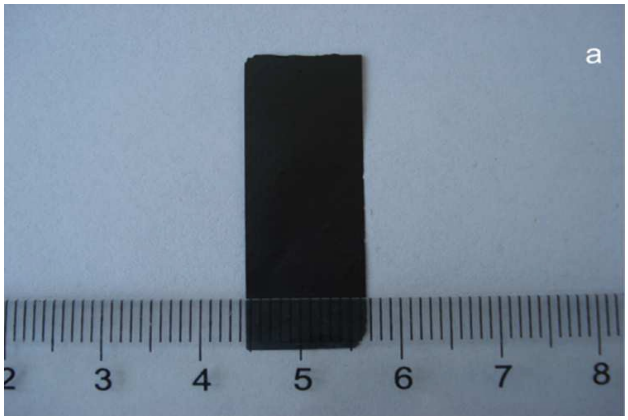

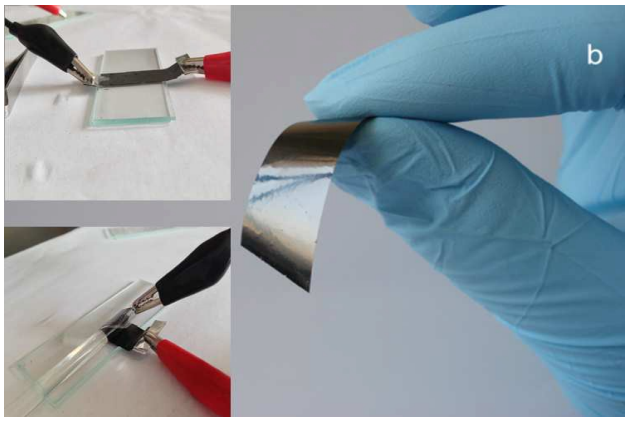

Fig. 2

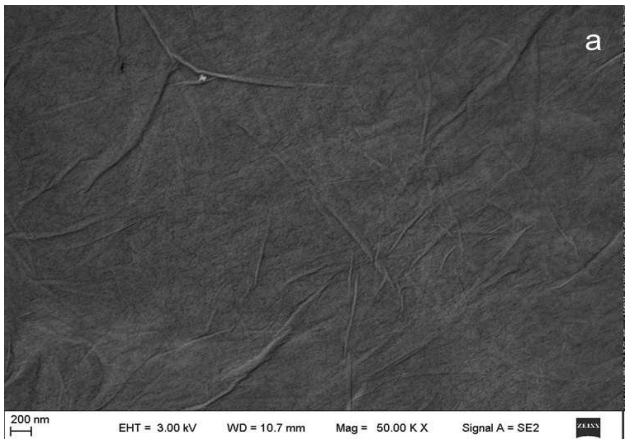

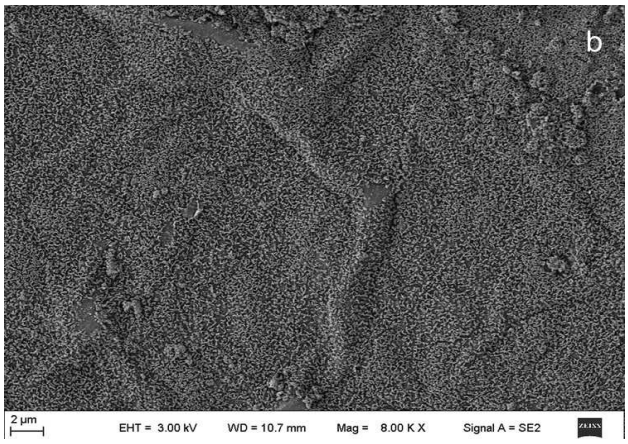

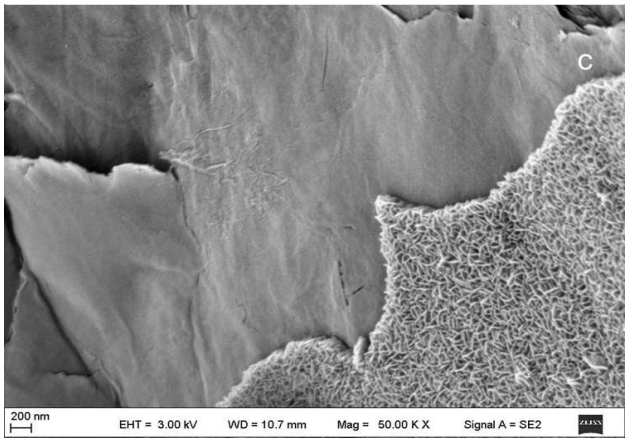

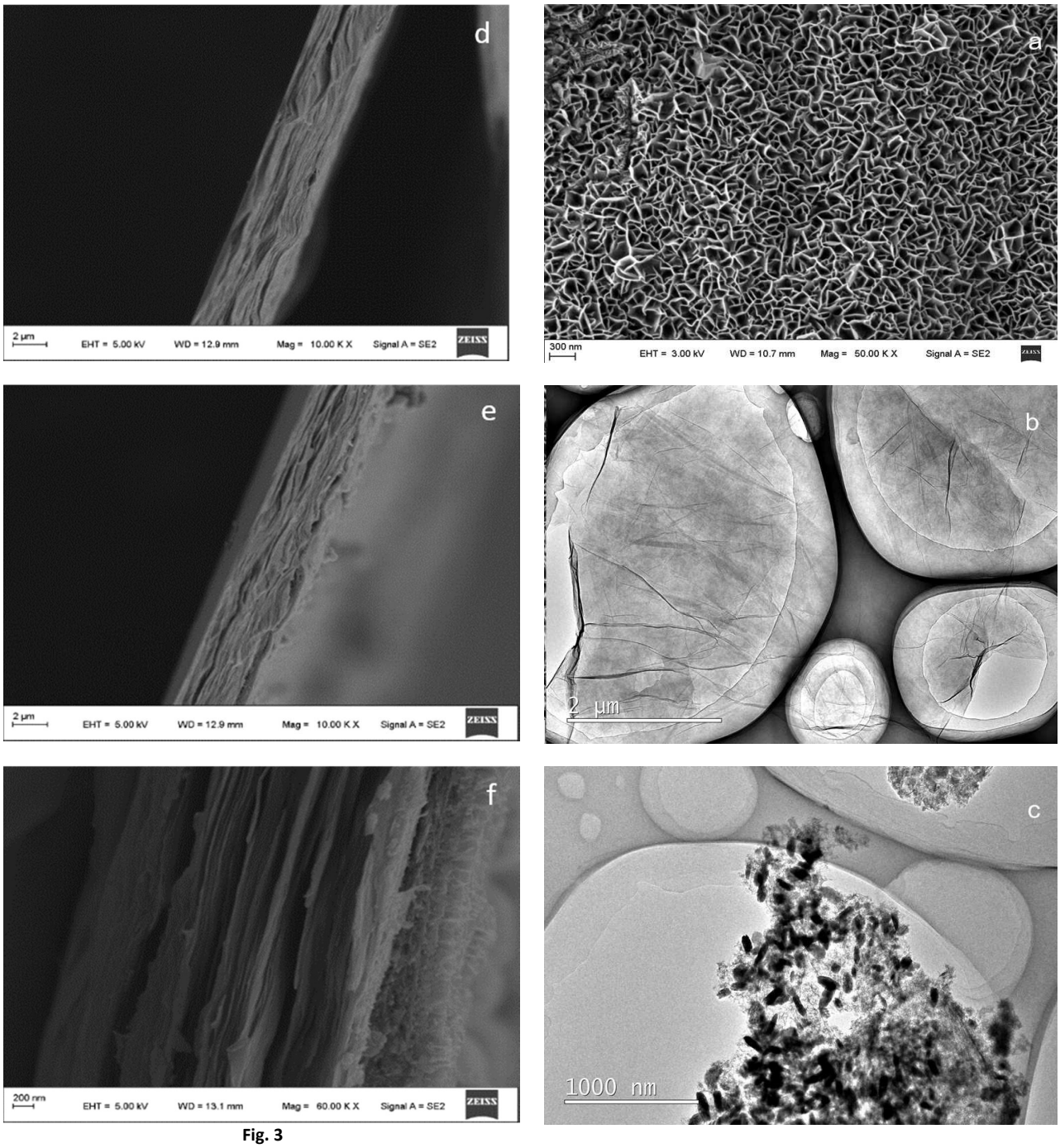

Fig. 3

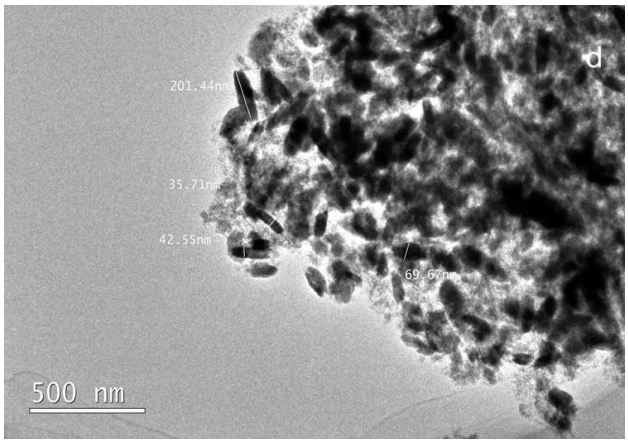

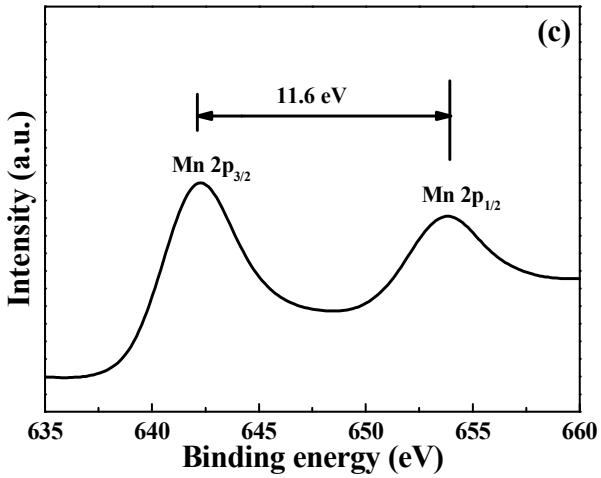

Fig. 4

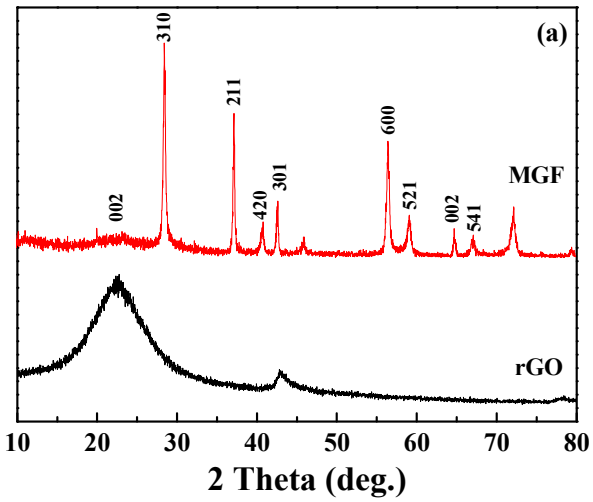

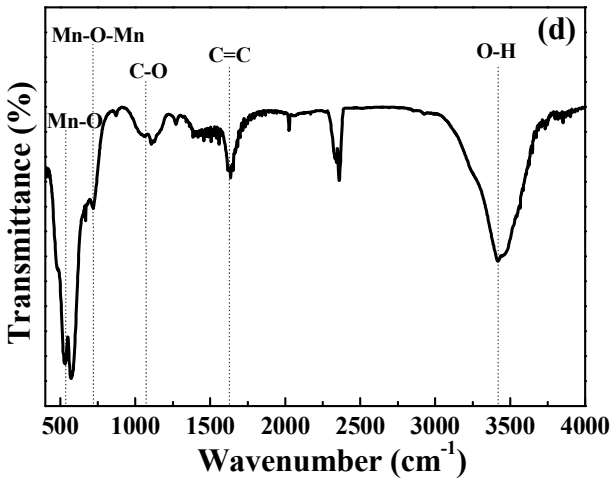

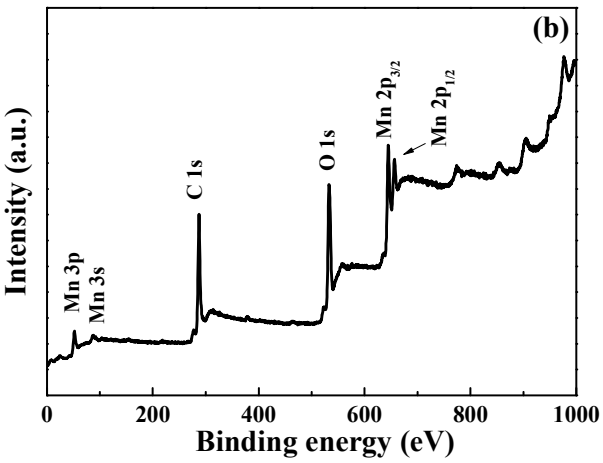

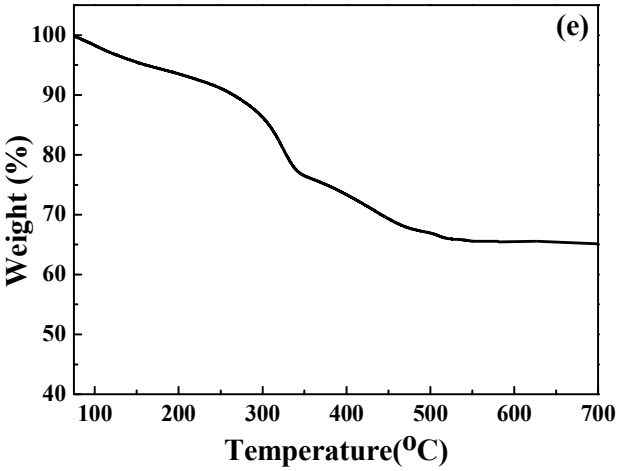

Fig. 5

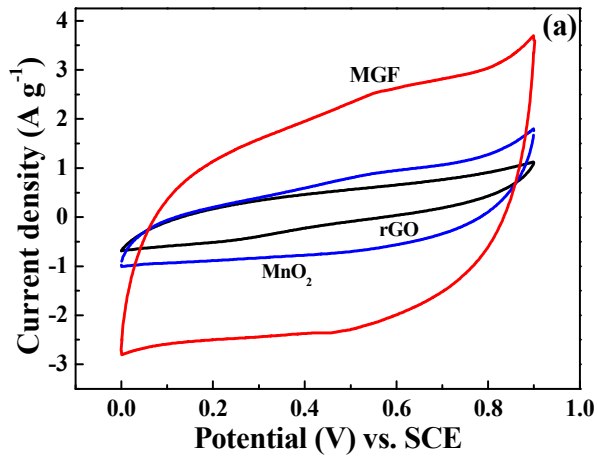

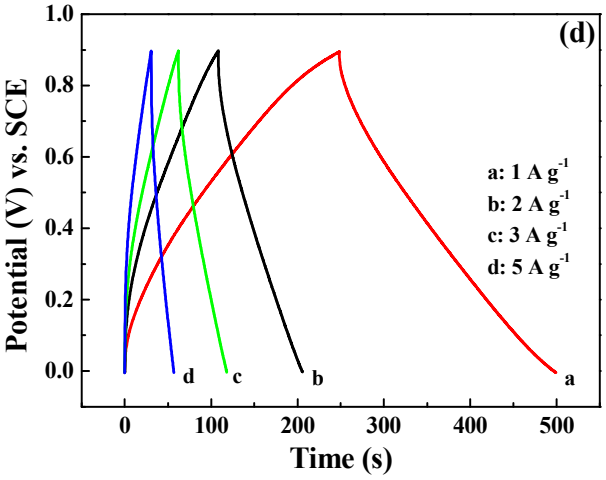

Fig. 6

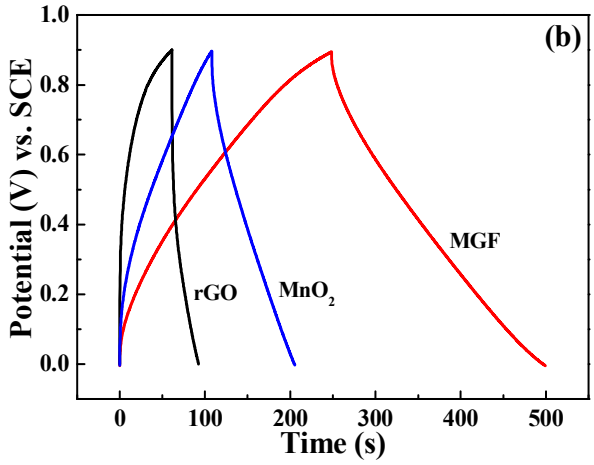

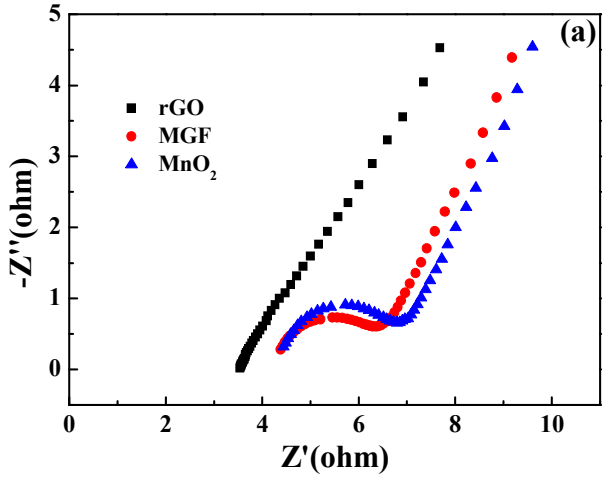

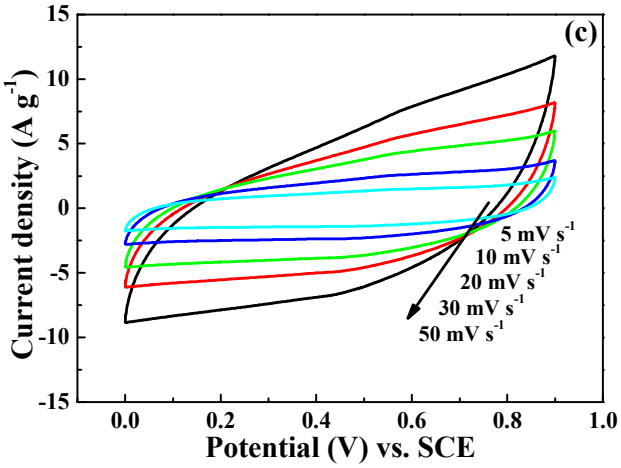

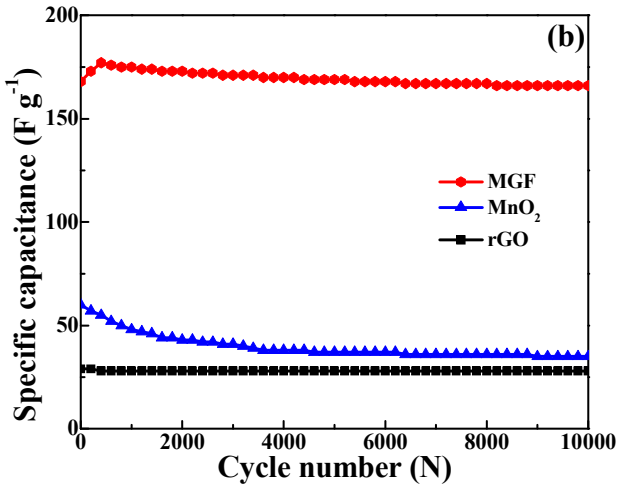

Fig. 7

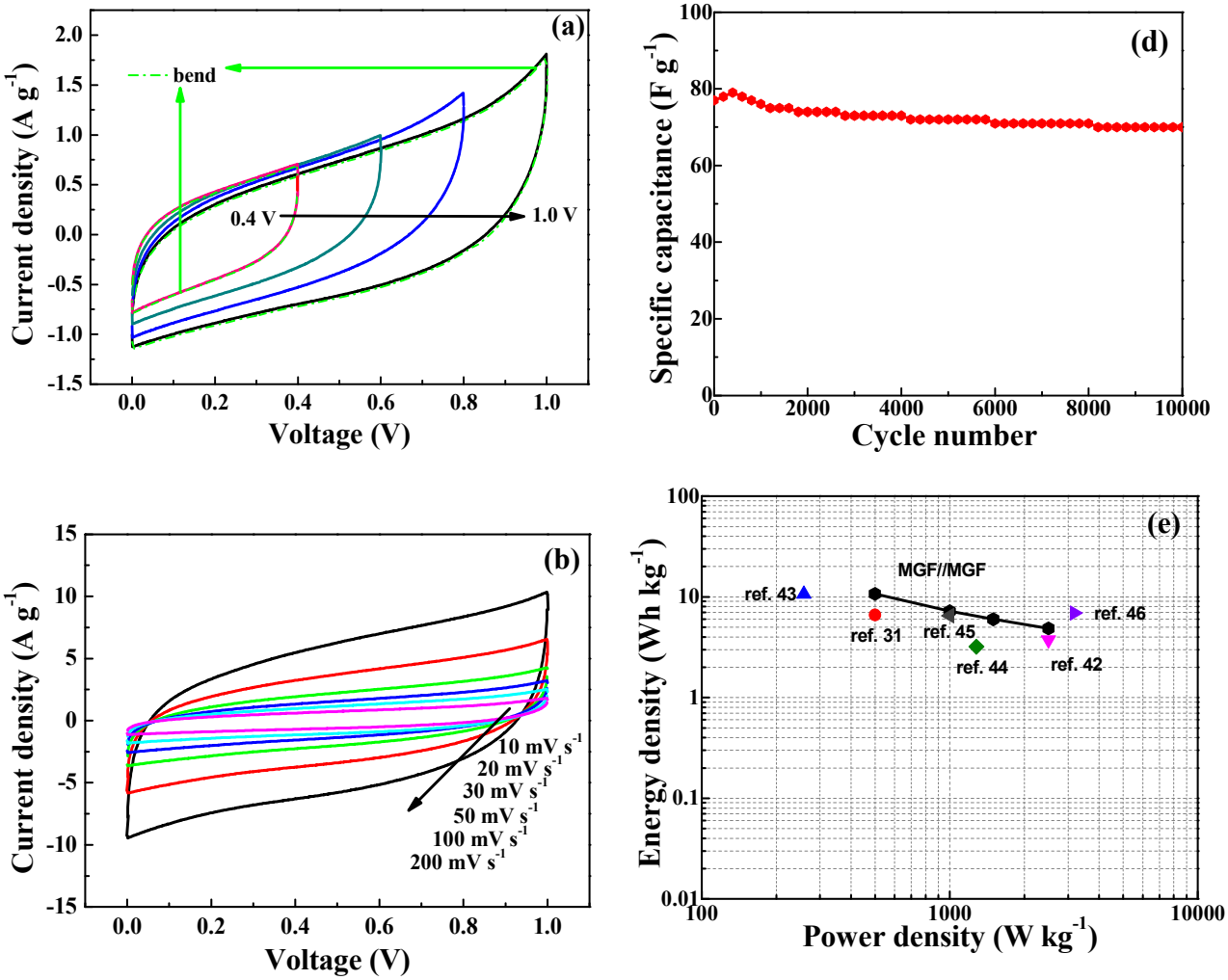

Fig. 8